Behavioral/Systems/Cognitive

Sleep Spindles in Humans: Insights from Intracranial EEG and Unit Recordings

Thomas Andrillon,[1,2]* Yuval Nir,[1]* Richard J. Staba,[3] Fabio Ferrarelli,[1] Chiara Cirelli,[1] Giulio Tononi,[1] and Itzhak Fried[3,4]

[1]Department of Psychiatry, University of Wisconsin–Madison, Madison, Wisconsin 53719, [2]Department of Cognitive Studies, École Normale Supérieure, 75005 Paris, France, [3]David Geffen School of Medicine, University of California-Los Angeles, Los Angeles, California 90095, and [4]Functional Neurosurgery Unit, Tel Aviv Medical Center and Sackler School of Medicine, Tel Aviv University, Tel Aviv 69978, Israel

Sleep spindles are an electroencephalographic (EEG) hallmark of non-rapid eye movement (NREM) sleep and are believed to mediate many sleep-related functions, from memory consolidation to cortical development. Spindles differ in location, frequency, and association with slow waves, but whether this heterogeneity may reflect different physiological processes and potentially serve different functional roles remains unclear. Here we used a unique opportunity to record intracranial depth EEG and single-unit activity in multiple brain regions of neurosurgical patients to better characterize spindle activity in human sleep. We find that spindles occur across multiple neocortical regions, and less frequently also in the parahippocampal gyrus and hippocampus. Most spindles are spatially restricted to specific brain regions. In addition, spindle frequency is topographically organized with a sharp transition around the supplementary motor area between fast (13–15 Hz) centroparietal spindles often occurring with slow-wave up-states, and slow (9–12 Hz) frontal spindles occurring 200 ms later on average. Spindle variability across regions may reflect the underlying thalamocortical projections. We also find that during individual spindles, frequency decreases within and between regions. In addition, deeper NREM sleep is associated with a reduction in spindle occurrence and spindle frequency. Frequency changes between regions, during individual spindles, and across sleep may reflect the same phenomenon, the underlying level of thalamocortical hyperpolarization. Finally, during spindles neuronal firing rates are not consistently modulated, although some neurons exhibit phase-locked discharges. Overall, anatomical considerations can account well for regional spindle characteristics, while variable hyperpolarization levels can explain differences in spindle frequency.

Introduction

Sleep spindles constitute an electroencephalographic (EEG) hallmark of non-rapid eye movement (NREM) sleep (Loomis et al., 1935; Andersen and Andersson, 1968; Achermann and Borbely, 1998; Destexhe and Sejnowski, 2001; De Gennaro and Ferrara, 2003; Steriade, 2003). In humans, spindles are classically defined as waxing-and-waning 10–16 Hz oscillations lasting 0.5–2 s (Gibbs and Gibbs, 1950). Comparable sleep spindles have been found in all tested mammalian species (Zepelin et al., 1994) and similar phenomena occur during barbiturate anesthesia (Contreras et al., 1997c) and *in vitro* (McCormick and Bal, 1997).

The neurophysiological mechanisms of spindle generation reflect the intrinsic properties and interactions between inhibitory cells in the thalamic reticular nucleus (RE) and bursting thalamocortical (TC) relay neurons (Steriade, 2000, 2003). The GABAergic neurons in the highly interconnected thalamic RE act as pacemakers and are both necessary and sufficient for spindle generation (Morison and Bassett, 1945; Steriade et al., 1985, 1987; Marini et al., 1992; Bal et al., 1995; Destexhe et al., 1998; Steriade and Timofeev, 2003; Halassa et al., 2011). Spindle waxing is attributed to gradual cell recruitment in RE-TC-RE loops (Steriade et al., 1993b; von Krosigk et al., 1993). The source of spindle waning and termination is less clear but possibly involves the depolarizing action of the thalamic I_H current and/or corticothalamic influence (Bal et al., 1995; Luthi and McCormick, 1998; Timofeev et al., 2001; Bonjean et al., 2011). Spindle synchronization is controlled by neocortical feedback, as decortication or spreading depression lead to asynchronous spindles (Contreras and Steriade, 1996; Contreras et al., 1997c).

Increasing evidence suggests that sleep spindles in humans are a diverse rather than prototypical phenomenon. One distinction involves fast (13–15 Hz) centroparietal versus slow (11–13 Hz) frontal spindles (Gibbs and Gibbs, 1950; Anderer et al., 2001; Schabus et al., 2007). Another distinction is between spindles that occur on a background of low-amplitude EEG in stage 2 sleep and are easily identified visually (Iber et al., 2007), and spindles associated with slow waves (Steriade et al., 1993a; Mölle et al., 2002). The functional role of spindles remains unclear, although they may play a role in memory consolidation (Schabus et al., 2004),

Received May 25, 2011; revised Oct. 17, 2011; accepted Oct. 19, 2011.

Author contributions: Y.N., C.C., G.T., and I.F. designed research; Y.N. and R.J.S. performed research; T.A. and Y.N. analyzed data; T.A., Y.N., R.J.S., F.F., C.C., G.T., and I.F. wrote the paper.

This work was supported by the Human Frontier Science Program Organization long-term fellowships (Y.N.), the Brainpower for Israel Fund (Y.N.), the NIH Director's Pioneer Award (G.T.), and NINDS grants (R.J.S., I.F.) We thank the patients for their cooperation; E. Behnke, T. Fields, A. Tankus, N. Suthana, and K. Shattuck for assistance with data acquisition and software; B. Salaz and I. Wainwright for administrative help; and S. Sarasso, V. Vyazovskiy, and B. Hung for discussions.

*T.A. and Y.N. contributed equally to this work.

The authors declare no conflicting financial interests.

Correspondence should be addressed to Dr. Yuval Nir, University of Wisconsin–Madison, School of Medicine, Department of Psychiatry, 6001 Research Park Boulevard, Madison, WI 53719. E-mail: ynir@wisc.edu.

DOI:10.1523/JNEUROSCI.2604-11.2011

 0270-6474/11/3117821-14$15.00/0

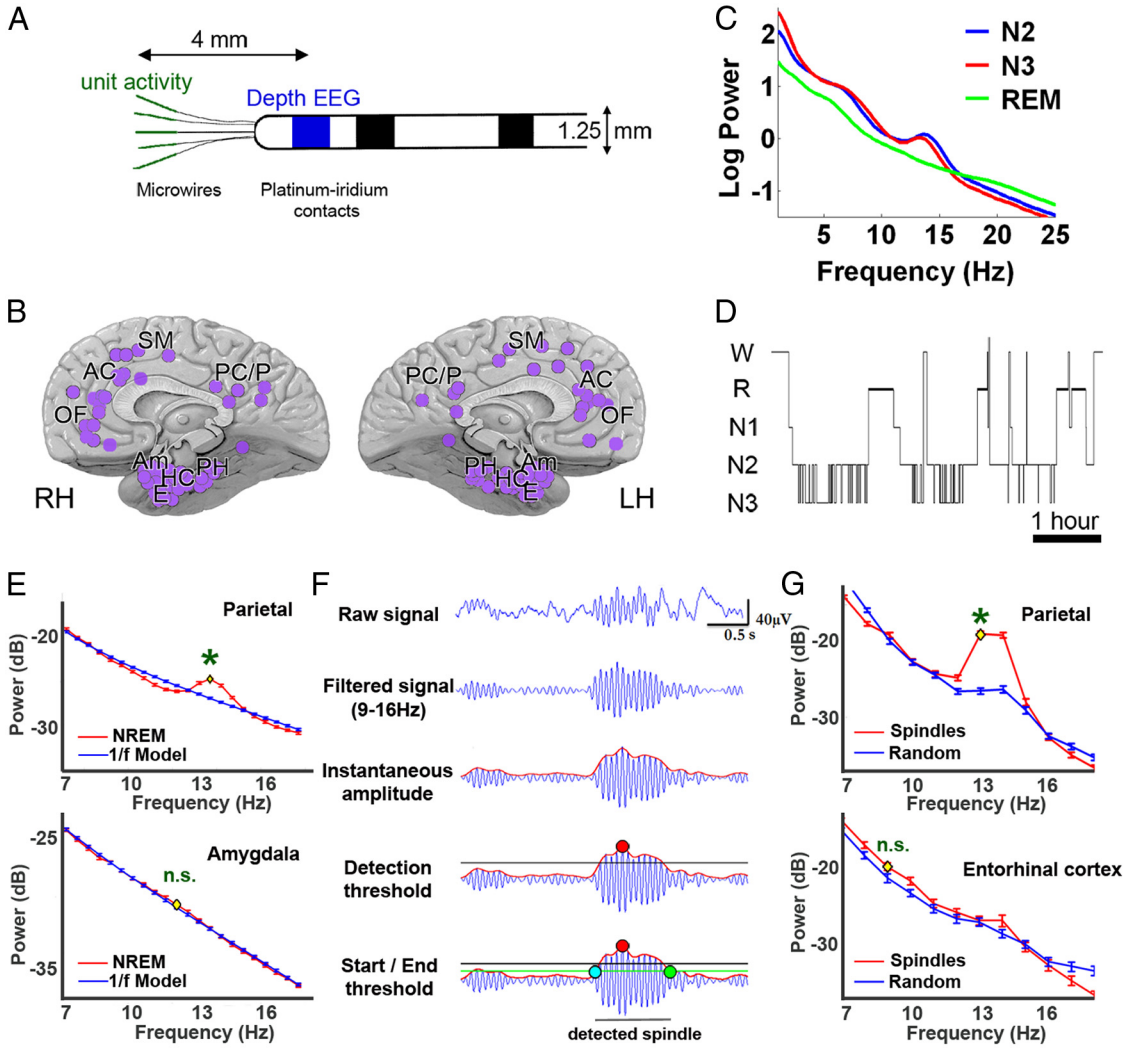

Figure 1. Data overview and spindle detection. ***A***, Illustration of flexible probes used for simultaneous recording of depth EEG (platinum contacts, blue) and unit activity (microwires, green). ***B***, Overview of 129 depth electrode locations in 13 individuals spanning multiple brain regions as seen from medial view. SM, Supplementary motor; PC/P, posterior cingulate/parietal cortex; PH, parahippocampal gyrus; HC, hippocampus; E, entorhinal cortex; Am, amygdala; LH, left hemisphere; RH, right hemisphere. ***C***, Example power spectra of scalp EEG in one representative individual in stage N2 sleep (blue), N3 sleep (red), and REM sleep (green). Note high power in slow-wave (<4 Hz) and spindle (9–16 Hz) range in NREM sleep. ***D***, Hypnogram: time course of sleep–wake stages in the same individual. W, Wake; R, REM sleep; N1–N3, NREM sleep, stages 1–3. ***E***, Spindle detection step 1: channels with spindle activity in NREM sleep are chosen for further analysis. Spectral profiles of a typical selected channel (parietal lobe, top) and a typical discarded channel (amygdala, bottom). For each channel, power in NREM sleep (red) was compared with a $1/f^{\alpha}$ model (blue), and channels with a significant peak (asterisks) in the range of 9–16 Hz are considered for further analysis. Yellow dots denote frequency with maximal power difference and error bars denote SEM across 10 s epochs of NREM sleep. ***F***, Spindle detection step 2: individual spindles were selected based on their power and duration. Raw EEG (top row) is filtered in the spindle range (9–16 Hz, second row). The instantaneous amplitude is extracted via the Hilbert transform (red trace, third row). A detection threshold is set at mean + 3 SD of spindle power across NREM sleep (horizontal black line, fourth row) and peaks exceeding this threshold (red dot) are considered putative spindles. A start/end threshold is set at mean + 1 SD of spindle power across NREM sleep (horizontal green line, bottom row), thereby defining start and end times (cyan and green dots, respectively) and determining spindle duration (between 0.5 and 2 s). ***G***, Spindle detection step 3: channels in which power increases of detected events were specific to the spindle range rather than broadband were chosen for final analysis. Spectral profiles of detected events in a typical selected channel (parietal lobe, top) and a typical discarded channel (entorhinal cortex, bottom). For each channel, power of detected events (red) is compared with power of random 1 s segments (blue), and channels with a significant peak which is specific to the spindle range (9–16 Hz) are chosen for final analysis. Note that detected events in entorhinal cortex had a diffuse broadband power increase. Yellow dots and error bars as above.

cortical development (Khazipov et al., 2004), regulation of arousal (Destexhe and Sejnowski, 2002), and in maintaining a disconnection from the external environment through a "thalamic gate" (Steriade, 2003). In addition, spindles have been recently explored as a potential biomarker for psychiatric disorders such as schizophrenia (Ferrarelli et al., 2010). To be able to identify the role(s) spindles could play during normal states of vigilance and to exploit them as a biomarker for pathology, it is necessary to first better understand spindle properties through a comprehensive investigation of their characteristics when they occur most prominently, i.e., human sleep. To this aim, here we characterize in detail sleep spindles in humans using simultaneous recordings of intracranial depth EEG and unit spiking activities in multiple brain regions in the cortex and hippocampus of 13 individuals undergoing presurgical localization of pharmacologically resistant epilepsy.

Materials and Methods

Subjects and polysomnographic sleep studies. Thirteen patients (6 males, 7 females) with pharmacologically intractable epilepsy (ages 19–52 years) underwent monitoring with depth electrodes (Fig. 1*A*) for seizure foci identification and potential surgical treatment (Fried et al., 1999). Pa-

tients provided written informed consent to participate in the research study, under the approval of the Medical Institutional Review Board at University of California, Los Angeles. Electrode location was based only on clinical criteria, and all surgery was performed by Itzhak Fried.

Sleep recordings were conducted 48–72 h after surgery, at a minimal interval of 12 h from identifiable seizures, and lasted for ~7 h between 11:00 P.M. and 6:00 A.M. In addition to continuous video monitoring, the montage included two electrooculogram (EOG), two electromyogram (EMG), and four scalp electrodes (positioned at C3, C4, Pz, Fz), as well as two earlobe electrodes for referencing. Sleep–wake stages were scored according to established guidelines (Iber et al., 2007).

Data acquisition. Electrode location varied between patients based on their clinical profiles. Electrodes were placed in frontal, parietal, and cingulate cortices, as well as temporal lobe regions such as hippocampus, amygdala, entorhinal cortex and parahippocampal gyrus (Fig. 1*B*). For each patient, 8–12 flexible polyurethane depth electrodes (1.25 mm diameter) were implanted orthogonal to the lateral surface of the skull with the distal tip of each electrode typically positioned in medial limbic brain structures. Each electrode position was identified using postimplant computed tomography coregistered with preimplant magnetic resonance imaging (Brain Navigator, Grass-Telefactor Corp.). Scalp and intracranial depth EEG data were continuously recorded, sampled at 2 kHz, bandpass-filtered in hardware between 0.1 and 500 Hz, and rereferenced offline to the mean signal of the earlobes electrodes.

Each depth electrode terminated in a set of eight insulated 40 μm platinum-iridium microwires (impedances 200–500 KΩ) (Fried et al., 1999) (Fig. 1*A*). Microwire signals were simultaneously recorded continuously (Cheetah Recording System; Neuralynx for 10 patients; Neuroport Recording System; Blackrock Microsystems for 3 patients), sampled at 28 kHz (10 patients) or 30 kHz (3 patients), bandpass filtered in hardware between 1 Hz and 9 kHz, and referenced locally to a ninth noninsulated microwire.

Detection of spindles and their separation from pathological events. Spindles were detected automatically following previously published algorithms (Clemens et al., 2007; Ferrarelli et al., 2007) based on a sequential three-step process (Fig. 1*E–G*) implemented in Matlab (MathWorks) as follows. First, to minimize false detections, only channels with robust spindle activity in NREM sleep were chosen for further analysis. In each individual channel, spindle (9–16 Hz) power in NREM sleep was compared with a fitted $1/f^{\alpha}$ model (both were estimated across multiple 10 s epochs) and channels with a difference that was statistically significant at $p < 0.001$ (unpaired t test for maximal peak) were further considered (Fig. 1*E*). Second, putative spindles were selected based on their power and duration. EEG signals were bandpass filtered between 9 and 16 Hz (−3 dB at 8.8 and 17.3 Hz) using a zero-phase fourth order Butterworth filter. The instantaneous amplitude was computed via the Hilbert transform and two thresholds were defined based on this amplitude time course across artifact-free sleep epochs. A detection threshold was set at mean + 3 SDs and amplitudes exceeding this threshold were considered potential spindles. A start/end threshold was set at mean + 1 SD and events whose duration was between 0.5 and 2 s were further considered (Fig. 1*F*). Detections within 1 s were merged as single events. Third, since transient events can introduce power increases across a wide range of frequencies including the spindle range (De Gennaro and Ferrara, 2003), only events in which power increases were specific to the spindle range rather than broadband were chosen for final analysis. For each channel, power of detected events was compared via an unpaired t test with power of random 1 s segments in NREM sleep (Fig. 1*G*). Channels exhibiting weaker diffuse broadband power increases ($p \geq 0.0001$ at maximal difference) were excluded. We further verified the spectral specificity of each spindle by excluding any detection that coincided with control events that were above mean + 5 SDs in the 20–30 Hz range.

Sleep spindles were separated from pathological interictal epileptiform events as follows. As was recently done for slow waves (Nir et al., 2011), epileptiform interictal spikes were separately detected automatically in depth EEG by high-pass filtering offline above 100 Hz and by identifying events whose amplitude exceeded mean + 5 SDs and whose duration was <70 ms (de Curtis and Avanzini, 2001). We verified visually that such automatic detection was effective in identifying interictal spikes in each channel separately. Based on this detection we discarded *post hoc* any putative spindles within ±1 s of interictal spikes. In addition, the parameters of the spindle detection algorithm (e.g., frequency range, filter settings, thresholds) were optimized after extensive visual inspection to minimize false detections of epileptiform activities as spindles, although a wide range of parameters yielded similar detections (data not shown). Naturally, the density and duration of spindles reported throughout the paper depend on the specific detection parameters used.

In the hippocampus, we visually selected for further analysis a subset of the automatically detected events that also exhibited a clear waxing-and-waning spindle shape. We computed in each hippocampal electrode separately the probability of such spindles to co-occur with detected events in other locations as p = number of concomitant spindles for a given pair of structures/number of hippocampal spindles.

Timing and frequency of spindles. For each detected spindle, several parameters were stored for further analysis including start and end times, frequency, and amplitude. The timing of individual spindles was determined as the mean of their start and end times (center), thereby avoiding influence by the choice of the start/end threshold.

The frequency of each detected spindle was estimated by computing the spectrogram in 10 s intervals (short-time Fourier transform, 744 ms window, 95% overlap) and identifying the maximal power for each event within the spindle frequency range with a resolution of 0.2 Hz. Next, distribution of spindle frequencies were computed per channel and later averaged for each brain region (Fig. 2*B*).

Spectral dynamics during individual spindles in specific regions (Fig. 2*C*) were evaluated by computing spectrograms (as above) in 2 s windows centered on the time of maximal amplitude. Differences in frequency between the beginning and end of spindles (Fig. 2*C*) were evaluated in each event separately by comparing the instantaneous frequency (in spectrograms) between start and end times via a paired t test ($\alpha = 0.05$).

Comparing timing and frequency across regions. For each pair of channels in the same individual, concomitant spindles were selected if there was temporal overlap in their occurrence. Both channels were considered as the "seed" and "target" alternatively and spectrograms (as above) were aligned to the time of maximal amplitude in the seed channel (Fig. 3*C*). For each spindle event separately, the timing of maximal amplitude and the frequency at maximal amplitude were compared across the two channels and the mean difference in timing and frequency across spindles was computed for each pair (Fig. 3). Next, electrode locations in frontal and parietal locations were grouped into 10 regions: bilateral orbitofrontal cortices, anterior cingulate cortices, presupplementary motor areas, supplementary motor areas, and posterior cingulate cortices (Fig. 3*B*). In 12 individuals in whom there was more than one such location, the typical delay between all pairs of spindles for any given pair of regions [e.g., left orbitofrontal cortex vs right posterior cingulate cortex (PC)] were averaged (Fig. 3*B*, edge color). Furthermore, each region was ranked in each individual from 0 (earliest detection) to 1 (latest detection) and such ranks were similarly averaged across individuals (Fig. 3*B*, node colors). We also examined whether the timing differences between regions (pooled in 50 ms bins) were proportional to frequency differences via linear regression (Fig. 3*D*).

Association of spindles with slow waves. Individual slow waves (positive and negative peaks in the EEG filtered below 4 Hz that were separated by 0.25–1 s) were automatically detected as described previously (Riedner et al., 2007) and separated from abnormal paroxysmal events (Nir et al., 2011). The highest amplitude waves in each channel (top 20%) were used to examine spindle occurrence ±2 s around down-states (depth-positive and surface-negative peaks) or up-states (depth-negative and surface-positive peaks) in 100 ms bins (Fig. 4*B*). Confidence intervals ($\alpha = 0.05$) were estimated by computing the mean and SD of spindle occurrence across the 4 s detection interval and significant deviations from chance were identified via a two-tailed t test for each time bin separately.

Local sleep spindles. For each detected spindle, we examined whether other channels recorded a spindle that temporally overlapped with the spindle in the seed channel, using each channel as seed in turn. The presence or absence of coincident spindles between channels was labeled "concordant" or "non-concordant," respectively (Fig. 5*B*). In both seed

and target regions we computed the spectral dynamics (spectrograms as above) in ±1 s intervals aligned to the peak spindle power in the seed channel. Spectrograms were normalized in each channel separately relative to power modulations in random intervals with no detected spindles in the seed channel (Sirota et al., 2003). Statistical comparison of spindle power in concordant and non-concordant cases was performed via a *t* test based on peak power. To determine the percentage of cases in which "entirely local" spindles occurred (i.e., seed channel showed detected spindle while nothing different from chance occurred in a target channel), we reduced our detection criteria (above) to include spindles that exceeded a confidence interval of 95% (rather than mean + 3 SD).

Dynamics of spindles throughout sleep. In a subset of five individuals exhibiting a clear homeostatic decline of slow-wave activity (SWA) during sleep, early and late NREM sleep were analyzed separately. We compared the density, frequency, amplitude, and locality of spindles between early and late NREM sleep via nonparametric Mann–Whitney *U* tests ($\alpha = 0.01$) separately for different spindle categories (e.g., all spindles, fast vs slow, frontal and centroparietal; Fig. 6*A*). The dynamics of spindle frequency within NREM sleep cycles was further examined. To this end, NREM sleep cycles were identified visually as continuous time intervals in NREM sleep preceding REM episodes ($N = 16$ cycles in 8 individuals). Figure 6*B* shows four of these NREM episodes (the third one being discarded since it is disrupted by a brief arousal). To compile results across individuals and cycles that varied in their duration, each cycle was divided into shorter epochs ($n = 10$ bins per sleep cycle) and the mean SWA and spindle parameters were computed for each bin (Fig. 6*C*). Bins were sorted based on their SWA and the frequency and density of spindles was compared across varying depths of sleep (as indicated by SWA levels).

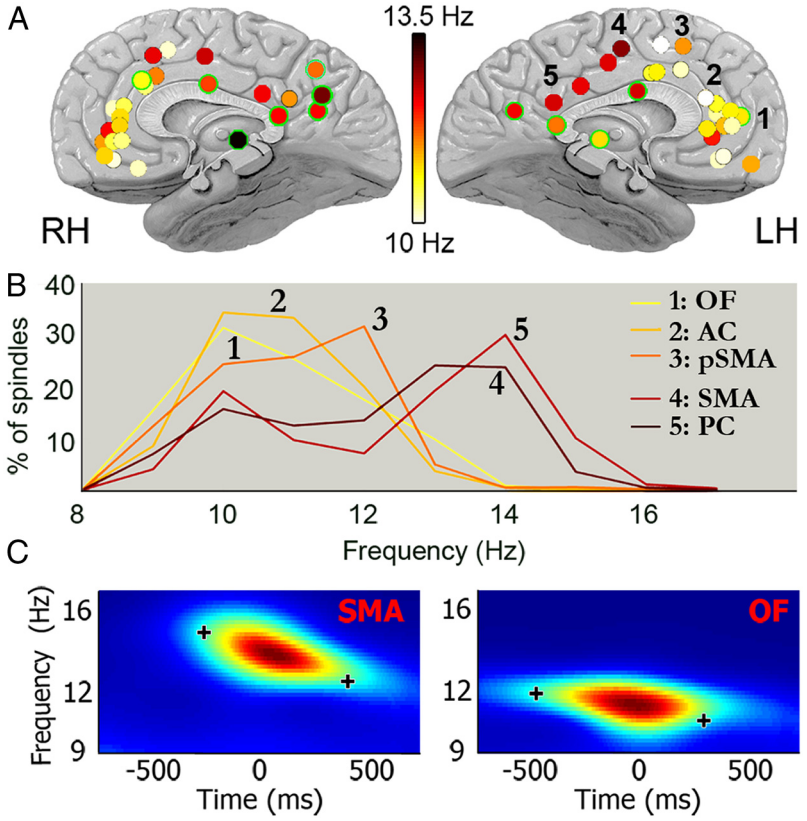

Figure 2. Fast centroparietal spindles differ from slow frontal spindles. ***A***, Average frequency of spindles across all depth electrodes ($n = 50$ electrodes in 13 individuals). The color of each circle denotes the mean spindle frequency in an individual electrode according to its precise anatomical location. Green outlines mark electrodes placed more laterally than the midline. Note the contrast between slow (9–12 Hz) frontal spindles and fast (13–16 Hz) centroparietal spindles. The two outliers in the medial prefrontal cortex (red circles) were the only electrode placements in one atypical individual in whom parietal spindles may be even faster. Numbers as in legend of ***B***. ***B***, Distribution of spindle frequencies grouped by region. Slow spindles are found in prefrontal regions (1–3) while fast spindles are found in centroparietal regions (4–5). Note the difference in spindle frequency between SMA and adjacent pSMA. ***C***, In each brain region, spectral frequency decreases during individual spindles. Spectrogram shows mean frequency dynamics in a representative centroparietal electrode in the SMA (left, $n = 159$ spindles) and in a frontal electrode in the OF (right, $n = 237$ spindles). Black crosses mark the mean instantaneous frequency around the beginning and end of spindles (13.8 and 12.5 Hz for fast spindles, 11.5 and 10.3 Hz for slow spindles). Note that frequency decreases during fast spindles and to a lesser degree during slow spindles.

Spiking activities during spindles. Units were identified using the wave_clus software package (Quiroga et al., 2004) as described previously (Nir et al., 2008). Briefly, a threshold was set at 5 SD above the median noise level of the high-pass filtered signal (>300 Hz), detected events were clustered using superparamagnetic clustering, and categorized as noise, single- or multiunit clusters. Classification of putative single units and multiunit clusters was based on the consistency of action potential waveforms, and by the presence of a refractory period for putative single units, i.e., <1% of interspike intervals (ISIs) within 3 ms. The stability of unit recordings was confirmed throughout long (~7 h) sleep recordings by comparing action potential waveforms and ISI distributions of detected units separately in 1 h intervals, and verifying that both waveforms and ISI distributions were indeed consistent and separable between different clusters throughout the night.

Neuronal action potential discharges recorded on individual microwires were examined in relation to sleep spindles detected in the depth EEG (macro-electrode ~4 mm away) in the same brain structure (Fig. 1*A*), as was recently done for slow waves (Nir et al., 2011). To quantify changes in firing rate during spindles, action potentials were binned in 100 ms bins ±2 s around the middle of each spindle. Confidence intervals ($\alpha = 0.05$) were estimated across the 4 s interval and significant deviations from chance were identified via a paired *t* test for each bin separately (Fig. 7*A*).

Phase-locked unit discharges during spindles (Fig. 7*B*) were examined as follows. Depth EEG was filtered in the spindle (9–16 Hz) range and individual spindles were detected as above. For each spindle, we extracted the instantaneous phase of the filtered EEG via the Hilbert transform. We examined the distribution of phase values at action potential times (Fig. 7*C*, "real distribution") and computed a *p*-value using Rayleigh's test for nonuniformity (circ_mean function, Circular Statistics Toolbox for Matlab). Since nonuniformity can be partially attributed to asymmetries in the EEG waveforms (Siapas et al., 2005), the critical *p*-values for significance were determined using bootstrapping for each unit separately as the 95th percentile after examining *p*-values across 1000 iterations while shuffling action potential timings within each segment (Fig. 7*C*, "shuffled spikes"). Finally, the preferred phase was determined for each phase-locked unit.

Statistical analysis. Error bars in figures denote SEM (SEM = SD/$\sqrt{(n-1)}$). Student's *t* tests were performed after confirming normal distributions via Kolmogorov–Smirnov tests or the Mann–Whitney *U* test (nonparametric) when normality could not be established.

Results

Polysomnographic sleep studies

Polysomnographic sleep studies were conducted in 13 neurosurgical patients with intractable epilepsy. Continuous overnight recordings lasted 421 ± 20 min (mean ± SEM). Polysomnography included EOG, EMG, scalp EEG, and video monitoring. Fig-

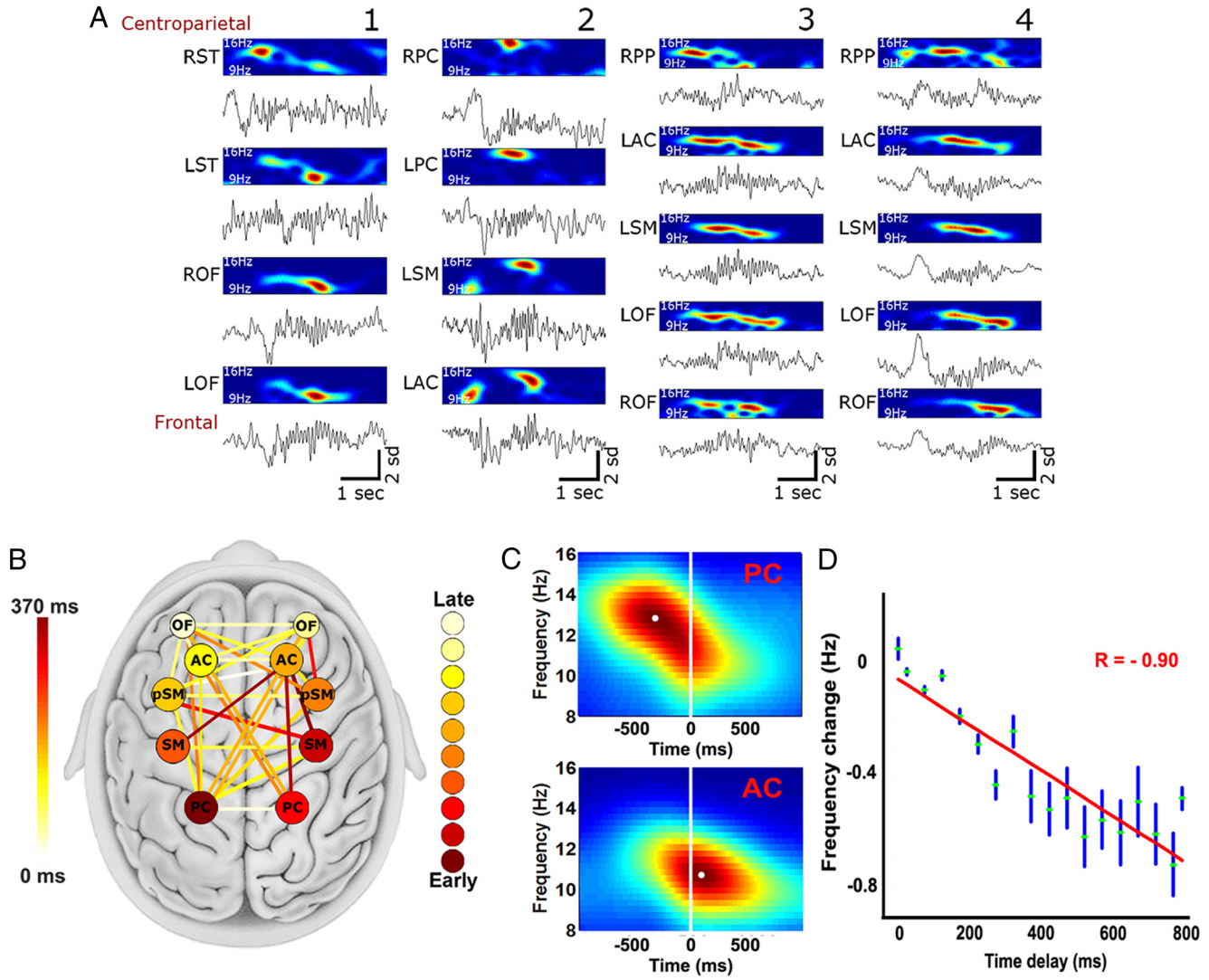

Figure 3. Fast centroparietal spindles precede slow frontal spindles. ***A***, Four examples of individual spindles in three individuals showing depth EEG along with corresponding spectrograms in the spindle range (9–16 Hz) during 4 s of NREM sleep. When spindles occur in multiple brain regions, fast centroparietal spindles precede slow frontal spindles. ***B***, Quantitative analysis of time offsets in spindle occurrence. A graph showing the order in which spindles are detected across multiple regions (node color) and the mean temporal delays between each pair of regions (edge color). Mean order and timing across spindles for all individuals ($n = 12$) indicate that centroparietal spindles precede frontal spindles. Abbreviations as in Figure 1. ***C***, An example of differences in timing and frequency between PC and AC in one individual. Spectrograms are aligned to the mean of peak power in AC and PC spindles. Note that AC shows a hint of an early fast component aligned with peak power in PC while its peak is at lower frequencies and delayed by >500 ms. ***D***, Frequency decreases (*y*-axis) and temporal delays (*x*-axis) are closely related in individual spindles ($r = -0.90$, $n =$ 9741 spindles in 50 electrode pairs).

ure 1*A–D* summarizes the experimental recording setup during sleep. Sleep–wake stages were scored following established guidelines as waking, NREM sleep stages 1 through 3 and REM sleep (Iber et al., 2007). Intracranial depth EEG was recorded in 129 medial brain regions bilaterally in frontal and parietal cortices as well as multiple limbic structures in the medial temporal lobe (Fig. 1*B*). While it should be noted that our sampling was mostly limited to medial brain areas, scalp topography suggests that human spindle activity is maximal at midline regions (Ferrarelli et al., 2007), thereby making our data particularly well suited to examine sleep spindles. We simultaneously recorded scalp EEG, depth EEG, and spiking activity from a total of 600 units (355 putative single units, 245 multiunit clusters).

Measures of overnight sleep in patients were in general agreement with typical findings in healthy young adults (Riedner et al., 2007). Sleep efficiency, time spent in different sleep stages, NREM-REM sleep cycles, and power spectra of scalp EEG resembled normal sleep characteristics. Moreover, in every subject, power spectra of scalp EEG data in NREM sleep (Fig. 1*C*) revealed robust slow-wave activity (<4 Hz) and spindle (9–16 Hz) power. These results indicate that sleep measures were similar to those of normal sleep in individuals without epilepsy.

Spindle occurrence across multiple regions in the human brain

Having characterized sleep using standard noninvasive polysomnography, we proceeded to identify individual spindles in NREM sleep in the scalp EEG and in the depth EEG of each brain region separately using an automatic algorithm (see Materials and Methods; Fig. 1*E–G*). Channels with robust spindle activity in NREM sleep (Fig. 1*E*) in which power increases of detected events were specific to the spindle range rather than broadband (Fig. 1*G*) were identified. Table 1 provides the results of spindle detection across multiple brain regions. In the scalp EEG, spin-

Table 1. Spindle occurrence across multiple regions in the human brain

Region	Number of channels with spindle detections		Density (spindles/min)	
Scalp				
Fz	12/13	(92%)	1.8	(±0.30)
C3–C4	22/26	(85%)	1.9	(±0.22)
Pz	12/12	(100%)	1.8	(±0.30)
	46/51	**(90%)**	**1.9**	**(±0.13)**
Frontal lobe				
Supplementary motor area	3/3	(100%)	1.2	(±0.49)
Orbitofrontal cortex	14/15	(93%)	2.2	(±0.24)
Anterior cingulate	14/16	(88%)	1.6	(±0.25)
Presupplementary motor area	4/7	(57%)	1.5	(±0.90)
Lateral frontal	2/4	(50%)	1.8	(±0.86)
	37/45	**(82%)**	**1.8**	**(±0.16)**
Parietal lobe				
Posterior cingulate	7/8	(88%)	1.1	(±0.29)
Posterior parietal	1/1	(100%)	2.2	(NA)
	8/9	**(89%)**	**1.3**	**(±0.29)**
Temporal lobe				
Temporal gyrus	4/6	(80%)	2.1	(±0.28)
Parahippocampal gyrus	11/16	(69%)	1.3	(±0.25)
Hippocampus	9/23	(44%)	1.1	(±0.13)
Entorhinal cortex	4/13	(31%)	0.74	(±0.11)
Amygdala	4/19	(21%)	0.89	(±0.18)
	32/79	**(41%)**	**1.2**	**(±0.12)**

Columns (left to right) show the brain region, the number of channels with spindle detections (over the total number of electrodes in that region), and the mean density of spindles per minute (±SEM across electrodes, $n = 13$ individuals). Note that while frontal and parietal regions showed robust spindle activity (comparable to scalp EEG channels), there was large variability in the occurrence and density of spindles in the medial temporal lobe.

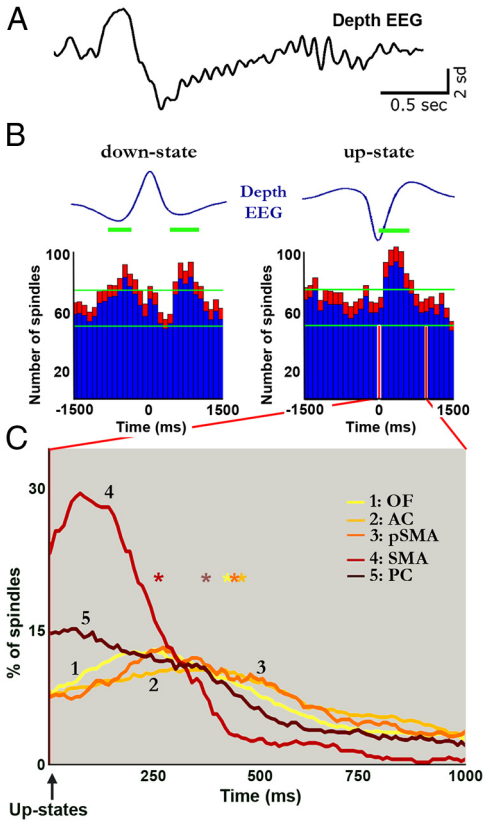

Figure 4. Association of spindles with slow-wave up-states. ***A***, Example of a single spindle associated with a slow-wave up-state as recorded in the depth EEG of the anterior cingulate cortex. ***B***, Number of detected spindles around slow-wave down-states (left, positive peaks in depth EEG) and up-states (right, negative peaks in depth EEG). Blue traces show average slow waves ($n = 13$ individuals). Red shading, SEM across channels; green horizontal lines, confidence interval ($\alpha = 0.05$). Thicker green bars, significant deviations from chance. Note that around slow waves, spindles occur more often after transition to the up-state. ***C***, Regional differences in association of spindles with slow-wave up-states. Note that fast centroparietal spindles (regions 4–5, red-brown colors) are more tightly associated with slow-wave up-states. Asterisks mark the average time to up-states for each region.

dles were robustly observed (90 ± 4.7% of electrodes showed spindle detections; mean ± SEM across individuals) and their density (1.9 ± 0.13 spindles/min) was consistent with densities reported in healthy individuals (Wei et al., 1999; Ferrarelli et al., 2010). Spindle density was significantly higher during sleep stage N2 than N3 (1.9 ± 0.14 vs 1.6 ± 0.14 spindles/min respectively, $p < 10 \times 10^{-3}$ via paired t test, $n = 46$ channels). In the depth EEG, frontal and parietal cortices exhibited robust spindle detections (82% and 89% respectively) with densities comparable to those observed in scalp EEG (1.8 ± 0.16 and 1.3 ± 0.29 spindles/min, respectively).

Spindle occurrence was further examined in the medial temporal lobe (MTL), where the presence of physiological spindles is still debated (Malow et al., 1999; Nakabayashi et al., 2001; Paré et al., 2002). The current results indicate reliable spindle occurrence in the parahippocampal gyrus (PHG, 69% of channels; 1.3 ± 0.25 spindles/min) and hippocampus (44% of channels; 1.1 ± 0.13 spindles/min), while spindle occurrence was lower in entorhinal cortex and amygdala (31% and 21% of channels; 0.74 ± 0.11 and 0.89 ± 0.18 spindles/min, respectively). Given the variability in spindle occurrence in the MTL that could be due in part to epileptogenicity, we analyzed spindles in MTL separately from spindles in frontal and parietal cortices, and present data from the MTL in the final section of the results.

Fast centroparietal spindles differ from slow frontal spindles

Since scalp EEG studies have long suspected a distinction between slow (11–13 Hz) and fast (13–16 Hz) spindles (Gibbs and Gibbs, 1950; Anderer et al., 2001; De Gennaro and Ferrara, 2003; Schabus et al., 2007), we computed the distribution of frequencies across all spindles in each channel separately across multiple brain regions (see Materials and Methods). In scalp EEG, centroparietal electrodes (C3, C4, Pz) showed a significant albeit diffuse dominance of fast spindles, whereas slow spindles prevailed in frontal derivations (Fz). Average spindle frequencies in Pz and Fz were 12.6 ± 0.23 Hz vs 11.3 ± 0.30 Hz, respectively (mean ± SEM across individuals) and these differences were statistically significant ($p < 0.01$, nonparametric Mann–Whitney U test across 24 channels). Next, the mean frequency of spindles was mapped across individual depth electrodes (Fig. 2*A*). In contrast to the small, yet statistically significant, differences in frequency observed with scalp EEG, the intracranial results reveal a topographical organization with a clear difference between fast (>12.5 Hz) centroparietal spindles and slow (<12.5 Hz) frontal spindles. "Centroparietal" was defined as brain areas from the supplementary motor area (SMA) proper back to posterior cingulate and parietal cortex, although some of these locations are in the frontal lobe. The distributions of spindle frequencies were averaged within and compared between the following five regions: orbitofrontal cortex (OF), anterior cingulate cortex (AC), pre-SMA (pSMA), SMA, and PC. The results (Fig. 2*B*) confirm the distinction between slow and fast spindles captured in part by scalp EEG. Furthermore, a difference between adjacent pSMA and SMA was observed in the same patient, and it nearly reached statistical significance across patients despite the limited sample (10.9 ± 0.72 Hz vs 12.6 ± 0.19 Hz respectively, $p = 0.057$, nonparametric Mann–Whitney U test, $n = 7$ channels) supporting

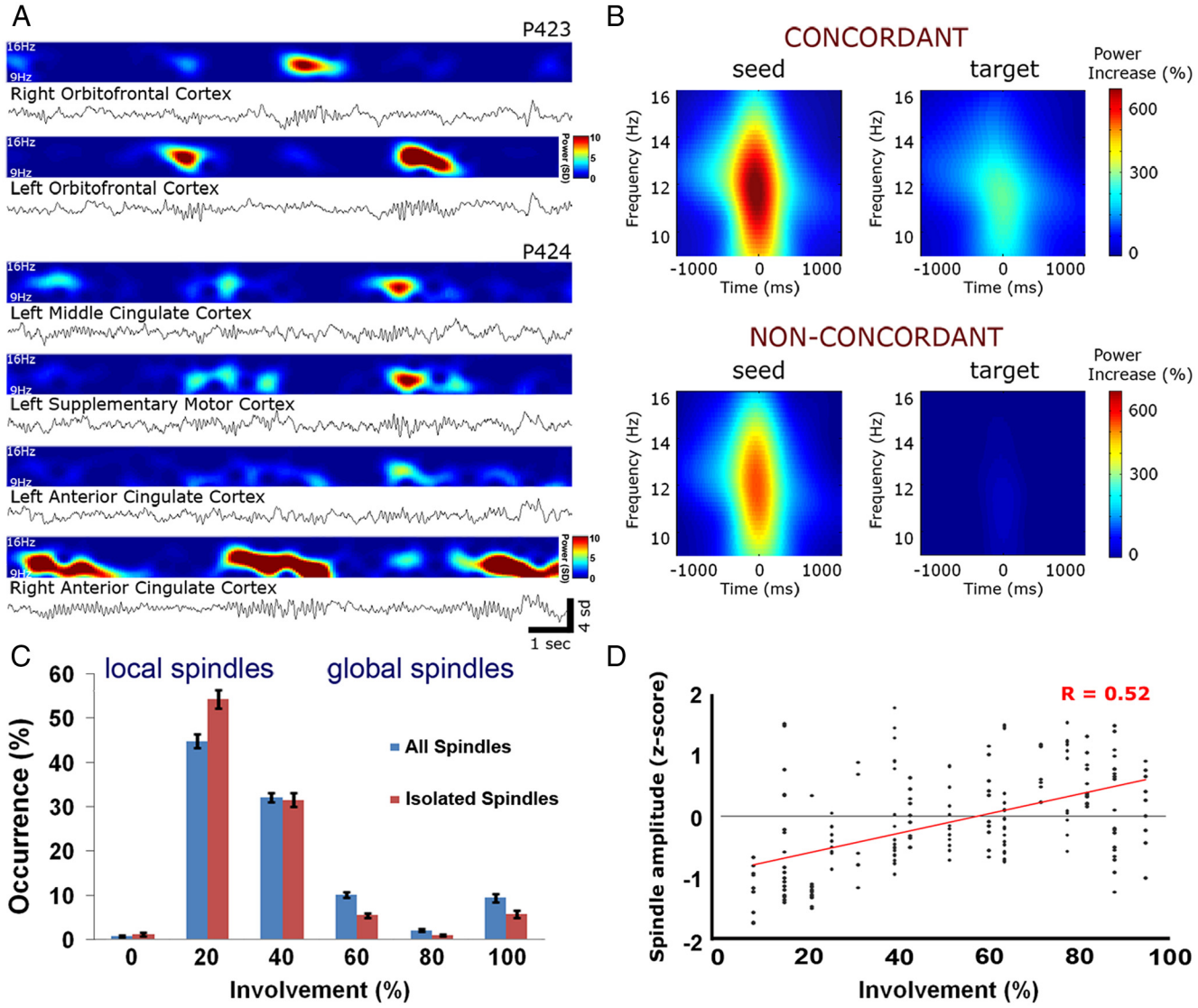

Figure 5. Local sleep spindles. ***A***, Two examples in two different individuals of depth EEG along with corresponding spectrograms in the spindle frequency range (9–16 Hz) during 15 s of slow-wave sleep. Note that regardless of slow waves, local spindles robustly occur without spindle activity in other regions, including homotopic regions across hemispheres and regions with equivalent signal-to-noise ratio showing the same global slow waves. ***B***, Quantitative analysis of spindle occurrence across pairs of channels. Top row (concordant spindles, 45% of cases) shows spectrograms for cases in which a spindle was detected in the seed channel as well as in the target channel ($n = 27{,}338$ in 170 pairs of regions in 12 individuals). Bottom row (non-concordant spindles, 55% of cases) shows spectrograms for cases in which a spindle was detected in the seed channel but not in the target channel ($n = 32{,}797$ in 170 pairs of regions in 12 individuals). Note that spindle power in non-concordant target channels is at near chance levels, indicating that our detection can reliably separate between presence and absence of spindle activity. ***C***, Most sleep spindles are local. Distribution of involvement (percentage of monitored brain structures expressing each spindle) for all spindles (blue bars, $n = 21{,}240$ spindles in 49 electrodes of 12 individuals) and for isolated spindles (red bars, spindles without a slow wave within $\pm$ 1.5 s, 37% of events). Note that 73% of spindles are observed in $<$50% of electrodes indicating that most spindles are local. ***D***, Scatter plot of spindle amplitudes as a function of involvement shows that global spindles have some tendency to be of higher amplitude ($r = 0.52$, $p < 0.0001$, $n = 170$).

the notion of two spindle groups rather than a continuous cortical gradient (see also Discussion). In addition, while frontal spindles were exclusively slow, centroparietal spindles had a bimodal distribution with a majority of fast spindles and fewer slow spindles, and this was also evident in the data of individual channels.

We also found that in the same brain region, frequency decreases during individual spindles. Figure 2*C* shows the average frequency dynamics in a representative SMA electrode (fast spindles, left) and an OF electrode (slow spindles, right). As can be seen, the instantaneous frequency of fast SMA spindles dropped on average from 13.8 to 12.4 Hz, and slow OF spindles showed a similar deceleration (from 11.5 to 10.4 Hz on average). A quantitative analysis across the entire dataset (2,851 fast and 10,607 slow spindles in 50 channels) revealed a significant decrease of -0.8 Hz/s in instantaneous frequency between spindle start and end times (-0.8 ± 0.04 Hz/s and -0.8 ± 0.02 Hz/s for fast and slow spindles, respectively, $p < 10 \times 10^{-12}$ between start and end times via two-tailed *t* test).

Fast centroparietal spindles precede slow frontal spindles

To further understand the distinction between fast centroparietal and slow frontal spindles, we examined whether these occurred independently or with consistent temporal relations. Figure 3*A* shows examples of individual spindles recorded simultaneously across several brain regions. As can be seen, fast centroparietal spindles occurred before slow frontal spindles, and the successive temporal occurrence across channels was accompanied by a decrease in spindle frequency. Next, a quantitative analysis of time

offsets across all pairs of brain regions was conducted and the order in which spindles appeared was computed (Fig. 3*B*). The results indicate that centroparietal spindles (in SMA and PC) occurred before slow frontal spindles (pSMA, AC, and OF) with a time difference of 203 ± 16 ms (mean ± SEM across 2024 pairs of spindles, $p < 10 \times 10^{-12}$ via one-tailed *t* test). Sorting regions according to the order in which their spindles were detected revealed that centroparietal regions typically preceded frontal locations (Fig. 3*B*). In contrast, within centroparietal regions and within frontal regions no significant time differences were found, supporting the notion of a discontinuous transition in timing and frequency between fast centroparietal and slow frontal spindles (see Discussion). Figure 3*C* provides an example of the average timing relation between all spindle pairs ($n = 139$) detected concomitantly in the PC and AC in one individual. As can be seen, timing and frequency differences appear closely linked. Indeed, across the entire dataset timing and frequency of spindles were found to be tightly related in pairs of regions such that larger frequency deceleration was associated with longer time delays (Fig. 3*D*, $r = -0.90$, $n = 9{,}741$ spindles). Overall, the reduction in spectral frequency with respect to time delay between spindles was −1.3 ± 0.5 Hz/s, and this negative rate was comparable to that found for spindles within the same regions.

Association of spindles with slow-wave up-states

Since spindles are often associated with slow-wave up-states (Steriade et al., 1993a; Steriade and Amzica, 1998; Mölle et al., 2002), we examined how this association may vary for different spindles detected across different brain structures. We have recently characterized in detail slow waves and underlying unit activities in the same dataset (Nir et al., 2011). Here we used the same automatic detection of large slow waves in each individual channel and examined the occurrence of spindles around positive and negative peaks in depth EEG, corresponding to down and up states, respectively. Figure 4*A* depicts an example of an individual slow wave detected in the anterior cingulate followed by a spindle, whereas Figure 4*B* presents the quantitative analysis of spindle detections in relation to slow waves across the entire dataset. Higher spindle occurrence (Fig. 4*B*, right) was found in the 0–500 ms interval following negative peaks in depth EEG (up states), in line with previous reports (Steriade et al., 1993a; Mölle et al., 2002).

Next, association of spindles with slow-wave up-states was compared between different brain regions in the 1 s interval immediately following the transition to up-states when spindle occurrence was maximal (Fig. 4*C*). Fast centroparietal spindles were found to be more tightly associated with up states compared with slow frontal spindles. Spindles exhibited the shortest delay with up-states in the SMA, the region where spindles were also detected earliest. More generally, typical time differences be-

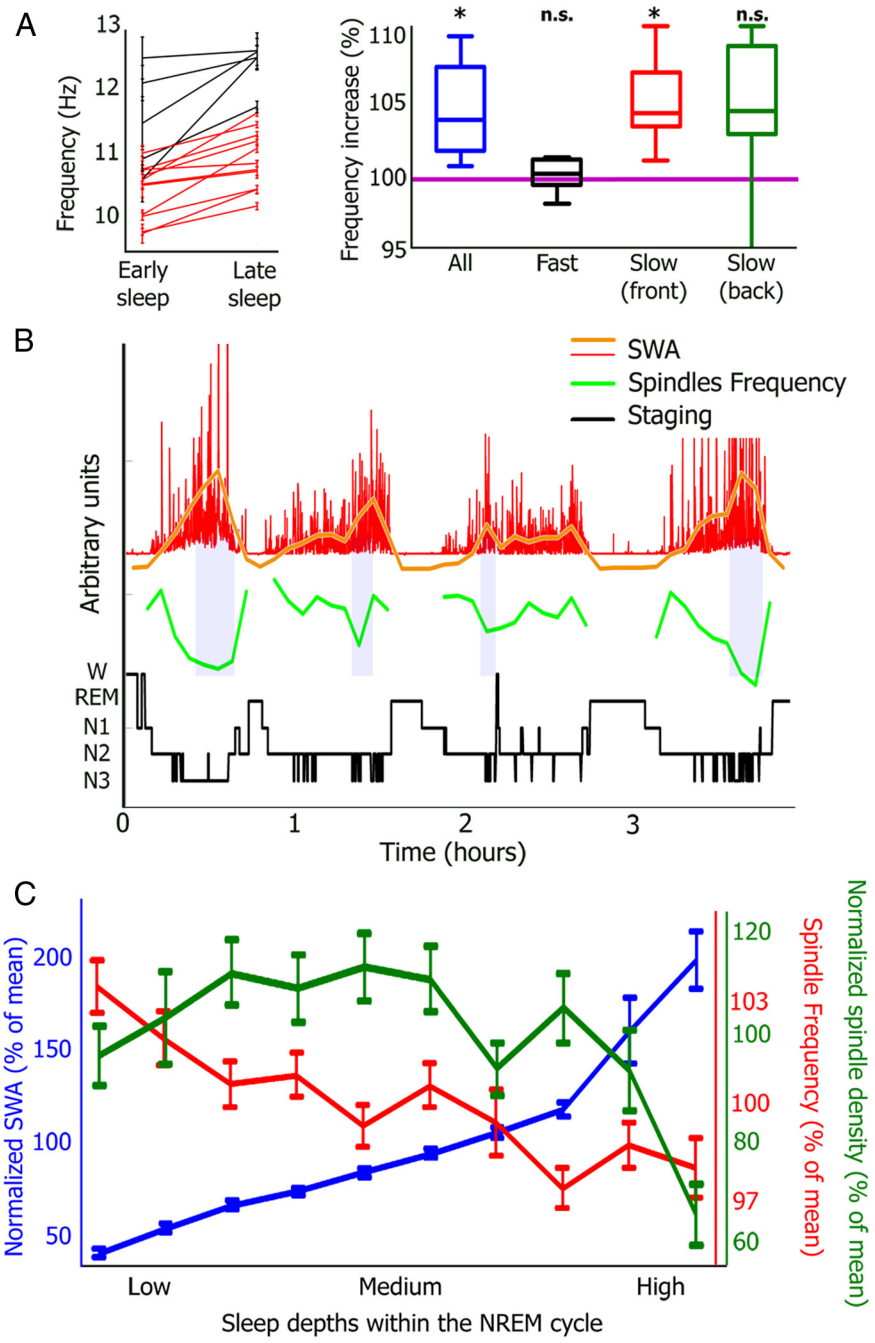

Figure 6. Deep sleep and high SWA are associated with lower spindle frequencies. ***A***, Frequency of slow spindle changes between early and late NREM sleep ($n = 5$ individuals, see Materials and Methods). Left, Frequency changes in centroparietal channels (black bars) and frontal channels (red bars). Right, Frequency changes for all channels (blue), fast spindles in centroparietal channels (black), slow frontal spindles (red) and occasional slow spindles in centroparietal channels (green). ***B***, Example of time course of SWA and spindle frequency dynamics throughout sleep in the anterior cingulate of one individual. Note that within NREM cycles, spindle frequency is lowest when SWA is highest (vertical purple bars) and increases toward transitions to REM sleep. ***C***, Quantitative analysis across the entire dataset ($n = 8$ individuals) comparing sleep depth (as measured by SWA, blue) with spindle frequency (red) and density (green). Note that deep sleep (high SWA on the right) is accompanied by fewer spindles ($r = -0.73$, $p = 0.02$) with lower frequencies ($r = -0.81$, $p = 0.005$). Error bars denote SEM across NREM sleep intervals ($n = 16$, see Materials and Methods).

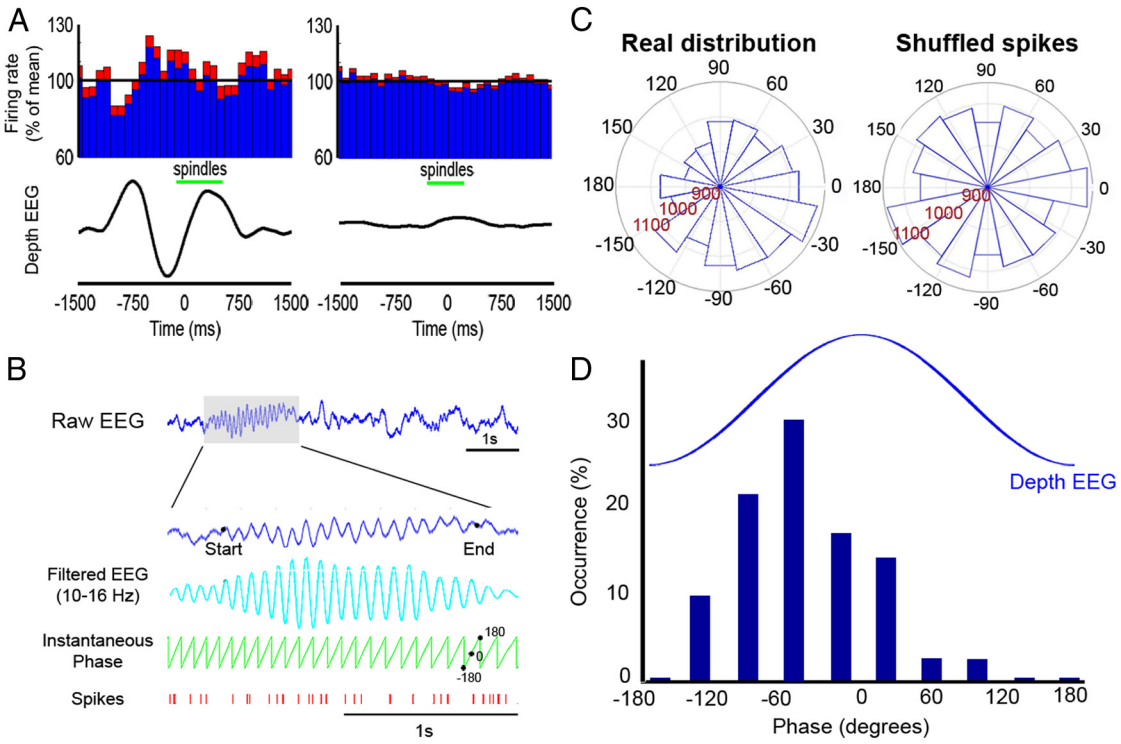

Figure 7. Unit discharges during sleep spindles. ***A***, Spindle-triggered averaging of unit spiking activity ($n = 207$ units), time locked to the middle point of the spindles in depth EEG ($n = 40$ channels). Left, Spindles occurring within 500 ms following up-states (8.5% of events). Right, All spindles. Red shades denote SEM across neurons. Black traces below bar graphs show the average depth EEG at those times. In contrast to robust firing rate modulations around transitions to UP states, firing rates modulations are largely absent during spindles. ***B***, Example of phase-locking analysis for one neuron and one spindle. For each detected spindle, raw depth EEG (blue trace) is filtered in the spindle range (9–16 Hz, cyan trace). The instantaneous phase is computed (green trace) and phase values are extracted for each action potential (red bars). ***C***, Phase-locking of spikes for the same unit displayed in ***A*** across all spindles (real distribution) and for spikes randomly shuffled within each spindle (shuffled spikes). A unit is considered phase-locked only if the Rayleigh p-value for its real distribution is smaller than the critical p-value defined as the 95th percentile across shuffled iterations. ***D***, Cumulative histogram of preferred firing phase for all phase-locked neurons ($n = 41/212$, 20% in 12 individuals). Note the tendency of phase-locked units to fire between the negative and positive peaks of spindles in the depth EEG.

tween regions were maintained for spindles associated with slow-wave up-states. Specifically, the average delays from negative peaks in the depth EEG to maximal spindle density in the SMA and PC were 267 ± 11 ms and 363 ± 11 ms, respectively, while frontal regions exhibited longer delays (AC, 460 ± 8 ms; OF, 425 ± 6 ms; pSMA, 449 ± 14 ms). The mean difference in delays between centroparietal and frontal sites was statistically significant ($p < 10 \times 10^{-12}$, unpaired two-tailed t test). Thus, the tighter association between centroparietal spindles and slow-wave up-states is consistent with their earlier occurrence compared with slow frontal spindles (see also Discussion).

Local sleep spindles

Although concomitant spindles were observed across multiple recording sites (above), we recently found that both sleep spindles and slow waves often occur independently in separate brain regions (Nir et al., 2011). We present these findings here as well to place them in the context of a comprehensive examination of sleep spindles in the human brain. Examination of local vs simultaneous spindles was performed only in cortical sites that had regular spindle occurrences, thereby excluding the possibility that local occurrence of spindles arises merely from their total absence in remote brain structures. Numerous examples of local sleep spindles occurring in specific brain regions were found (Fig. 5*A*). Local spindles occur without spindle activity in other regions, including homotopic regions across hemispheres and regions with equivalent signal-to-noise ratio showing global slow waves. We set out to quantitatively establish to what extent local sleep spindles occur across the entire dataset. We determined for each spindle in a given region whether spindles were present or not in other brain structures (Materials and Methods). The spectral power changes in concordant sites (45% of cases where a spindle was detected in both seed and target channels, Fig. 5*B* top row) were compared with those at non-concordant sites (55% of cases where a spindle was detected in the seed channel but not in the target, Fig. 5*B*, bottom row). The results revealed a clear difference between peak spectral power values of concordant and non-concordant conditions across spindles in target channels ($p < 10 \times 10^{-48}$, paired t test), indicating significant differences in underlying neuronal activity, and that non-concordant cases are indeed local spindles. Furthermore, the analysis of those cases where target channels did not exhibit any increase in spindle spectral power above the noise level (Materials and Methods) revealed that 32% of all non-concordant cases were local in the strongest sense, i.e., a full-fledged spindle was detected in the seed channel while spectral power in the target channel was not different from chance. Importantly, the occurrence of local spindles was independent of local slow waves, since "isolated" spindles without a slow wave within ± 1.5 s (35% of all spindles) were likewise mostly local (Fig. 5*C*). In addition, comparing homotopic regions revealed that 36 ± 2% of spindles were observed only in one hemisphere (mean ± SEM across 12 pairs), indicating that differences between anterior and posterior regions could not account for spindle locality.

Next, we quantified the involvement of multiple regions in spindles by computing the number of brain areas in which spindles were observed. The majority of sleep spindles involved a

limited number of brain regions (Fig. 5*C*), indicating that local spindles were more frequent than global spindles. Mean involvement in individual spindles was 48 ± 0.7% of monitored brain regions (mean ± SEM across 49 depth electrodes), indicating that most spindles were predominantly local. Finally, the spatial extent of spindles correlated with spindle amplitude (Fig. 5*D*, $r = 0.52$, $p < 0.0001$, $n = 212$).

Deep sleep is associated with lower spindle frequencies

The variability in spindle spectral frequency between brain structures and during individual spindles described in the preceding paragraphs could be due to changes in levels of thalamocortical polarization. Since the degree of thalamic hyperpolarization dictates the period of spindle oscillations (McCormick and Bal, 1997; Steriade, 2003), we hypothesized that spindles during deep sleep (early in the night or in the middle of NREM cycles when SWA is highest), would contain lower spectral frequencies than spindles during lighter sleep (late in the night or closer to REM transitions when SWA is lower).

To examine this possibility, we first compared spindle frequencies in five individuals showing a typical homeostatic decline of SWA, i.e., a progression from deep early sleep with powerful slow waves to lighter sleep late in the night. Spindle frequency was significantly lower in early deep sleep when SWA was highest (Fig. 6*A*, reduction of 0.63 ± 0.12 Hz, mean ± SEM across 16 channels, $p = 0.0004$, nonparametric Mann–Whitney *U* test). The modulation of spindle frequency in early vs late sleep was specific to slow spindles ($p = 0.002$ for slow frontal spindles vs $p = 0.62$ for fast spindles, Mann–Whitney *U* test).

Along the same line, spindle frequency changed within NREM cycles in accord with changes in SWA. Figure 6*B* shows an example of dynamics in spindle frequency and SWA across sleep in one individual, illustrating that in the middle of each NREM cycle when SWA was highest, spindle frequency was lowest. Next, this relation was examined in all NREM cycles followed by REM epochs (16 cycles in 29 depth EEG channels and 8 individuals, see Materials and Methods). Each NREM cycle was divided into 10 intervals with equal duration and SWA, spindle frequency and spindle density were computed separately for each interval (Fig. 6*C*). Both spindle frequency and spindle density were negatively correlated with SWA during NREM episodes ($r = -0.81$, $p = 0.005$, and $r = -0.73$, $p = 0.02$). These results indicate that deeper sleep and higher SWA are associated with lower spindle frequencies and fewer events.

Neuronal discharges during sleep spindles

Given that spiking activity across the human brain is tightly locked to EEG slow waves (Nir et al., 2011) we examined whether cortical neurons consistently modulated their firing rate during spindles. Examination of firing rates in putative single units from individual subjects revealed little evidence for consistent modulations in relation to spindles. On average across all 207 cortical units, we found that spindles occurring within 500 ms of transitions from inactive to active (UP) periods (8.5% of events) were accompanied by robust firing rate modulations (Fig. 7*A*, left), as expected (Nir et al., 2011). In contrast, when considering all spindles ($n = 63{,}724$) firing rate modulations were largely absent (Fig. 7*A*, right), although a small (~4%) yet significant reduction in neuronal discharges was observed 100–400 ms following the middle point of spindles, likely reflecting a diffuse tendency for an inactive (DOWN) state to occur at that time.

Next, we evaluated the phase-locking of unit discharges during spindles to determine whether units preferably fire at a specific phase of spindle oscillations (Fig. 7*B*). Figure 7*C* presents an example unit in which spikes preferably occurred at a particular phase (−30°) during spindles. Overall, 19.5% of neurons showed significant phase locking ($p < 0.05$, see Materials and Methods) with a tendency to fire more at the ascending phase of the spindle oscillation (preferred phase = −35 ± 8.5°, SEM across units) as measured with depth EEG (Fig. 7*D*).

On average, phase-locked units had a higher firing rate than the average firing rate (5.9 ± 1.2 Hz vs 3.1 ± 0.3 Hz, $p = 0.004$, Mann–Whitney *U* test for putative single units). It could be argued that the firing of many neurons is phase-locked during spindles, but only high firing rate neurons allow enough statistical power to reveal this phenomenon. However, 46% of phase-locked neurons had firing rates that were below the mean rate across the entire population. Alternatively, higher firing rates in phase-locked units may reflect a bias toward specific cell types such as interneurons (see also Discussion).

Spindles in the medial temporal lobe

Spindle occurrence in the MTL and its possible relation to pathology in epilepsy patients is a matter of continued debate (Malow et al., 1999; Nakabayashi et al., 2001; Paré et al., 2002). Our results (Table 1) revealed reliable spindle occurrence in the PHG, a dependable albeit lower occurrence in the hippocampus, and lower spindle occurrence in the entorhinal cortex and amygdala. Could such events reflect epileptiform activity? To address this, spindle detections in MTL were further analyzed in relation to the seizure onset zone (SOZ) based on the medical records of the patients. We examined whether inclusion in the epileptic focus (25 of 64 MTL channels) could predict spindle detection and spindle density in each region separately. If spindles recorded in MTL solely reflect abnormal activity, then it might be expected that the number of channels and rates of spindles would be higher inside than outside the SOZ, spindles in hippocampus would occur more regularly with spindles in adjacent MTL than remote neocortical sites, or unit firing would be more strongly correlated with MTL than neocortical spindles. Analysis found that in PHG and hippocampus, the majority of channels where spindles were recorded were outside the SOZ (64% and 63% respectively), and there was a trend for higher rates of hippocampal spindles outside than inside the SOZ (1.1 vs 0.8 spindles/min outside and inside the SOZ, respectively). In the entorhinal cortex and amygdala, spindle occurrence was comparable within and outside the SOZ. In addition, we found that detected events in hippocampus (Materials and Methods) co-occur more often with frontal/parietal spindles (remote from the SOZ) than with events detected in amygdala or entorhinal cortex ($p < 0.05$, Mann–Whitney *U* test). Finally, analysis did not find a stronger correlation between unit discharges and spindles in MTL than neocortical sites. It should be noted that due to possible volume conduction and lack of clear firing rate modulations our results cannot resolve the long-lasting controversy of potential epileptiform nature of hippocampal spindles. Nevertheless, these results indicate that although MTL spindles are less frequent and more variable, PHG and hippocampus can exhibit physiological spindles that may transcend possible links to pathology.

Sleep spindles and epilepsy

Our data were recorded in medicated epilepsy patients in whom epileptiform events during seizure-free periods (i.e., interictal episodes) may affect sleep, and sleep spindles in particular (Diner and Lüders, 2001; Steriade, 2005). Therefore, it was impera-

tive to confirm that our results could be generalized to the healthy population, and multiple observations strongly suggest that this is the case. First, overnight recordings were performed before routine tapering of anti-epileptic drugs to ensure a less significant contribution of epileptiform activities. Second, sleep measures were within the expected normal range, including distribution of sleep stages, NREM-REM cycles, and EEG power spectra of each sleep stage. Third, we specifically detected paroxysmal discharges and separated them from physiological sleep spindles, and we also confirmed that pathological events were not falsely detected as spindles through extensive visual inspection of each individual's data (Materials and Methods). Fourth, the occurrence rate of paroxysmal discharges was highly variable across channels, limited in its spatial extent, and entirely absent in some channels. By contrast, all the results reported here could be observed in every individual despite highly idiosyncratic clinical profiles. Fifth and most importantly, previous analysis revealed significant firing rate modulations in the same neurons during paroxysmal discharges (Nir et al., 2011), whereas unit discharges were not robustly modulated during sleep spindles, attesting to a good separation between pathological and physiological spindles. Since interictal EEG spikes and sleep spindles may be confounded in a more complex manner in the MTL, we adopted a conservative approach and analyzed those spindles separately from data obtained in frontal and parietal cortices based on a visual detection. Overall, we are confident that the current results can be generalized to individuals without epilepsy.

Discussion

Spindle occurrence and thalamic projections

Spindles were observed most frequently in neocortical regions, less often in the hippocampus and parahippocampal gyrus, and rarely in amygdala and entorhinal cortex (Malow et al., 1999; Nakabayashi et al., 2001; Paré et al., 2002; Sirota et al., 2003; Clemens et al., 2011). Such regional differences are consistent with the extent of thalamic projections to these structures. For example, many thalamic nuclei that are reciprocally connected with the RE project robustly to frontal and parietal cortices where spindles are abundant. By contrast, dorsal thalamic nuclei projecting to the MTL (where spindles occur less frequently) are not reciprocally connected with the RE in cats (Steriade et al., 1984; Paré et al., 1987; Jones, 2007). The lack of spindles in amygdala is consistent with sparse thalamocortical projections that only target the lateral nucleus (Jones, 2007). The difference in spindle occurrence between the hippocampus and entorhinal cortex is less clear and could reflect variability in recording from different layers in these structures.

Slow and fast spindles

Our intracranial results confirm and refine the distinction between slow (9–12 Hz) frontal and fast (13–16 Hz) centroparietal spindles (Loomis et al., 1935; Jankel and Niedermeyer, 1985; Jobert et al., 1992; Anderer et al., 2001; De Gennaro and Ferrara, 2003; Nakamura et al., 2003; Clemens et al., 2011). We find that (1) this distinction is present in each individual (2) spindle frequency shows a sharp transition between SMA and pSMA, (3) centroparietal spindles show a bimodal distribution whereas frontal spindles are exclusively slow, (4) frontal spindles often have frequencies as low as 9–10 Hz.

What gives rise to slow and fast spindles? Since spindles arise from RE-TC-RE loops, and because TC projections from different nuclei terminate in cortical regions that exhibit slow vs fast spindles, differences in spindle frequency could reflect the preserved topographical organization between thalamic nuclei and subregions in the RE sheet (Guillery and Harting, 2003; Steriade and Timofeev, 2003; Jones, 2007; Lam and Sherman, 2011). Posterior and lateral dorsal nuclei project to centroparietal cortex, whereas ventral and anterior dorsal nuclei mainly project to prefrontal regions (Jones, 2007; Cappe et al., 2009; Zhang et al., 2010). Some anterior nuclei project diffusely along the cingulate cortex (Jones, 2002) and could explain occasional slow centroparietal spindles. Finally, the difference in spindle frequency between SMA and pSMA suggests that these adjacent cortical regions receive input from different thalamic nuclei (Akkal et al., 2007).

Faster spindle frequencies are associated with earlier time onsets

Fast centroparietal spindles precede slow frontal spindles with a significant difference between adjacent SMA and pSMA, as was the case for spindle frequency. Differences in spindle timing and frequency are correlated across regions in individual spindles. Furthermore, within each brain region spindles decelerate such that frontal spindles show a hint of an early fast component aligned with centroparietal spindles and vice versa. Thus, individual spindles exhibit different frequencies and timings in distinct regions.

Differences in spindle timing and frequency were noted previously, but their close relation during individual spindles had yet to be established (Zygierewicz et al., 1999; Anderer et al., 2001; Nakamura et al., 2003; Dehghani et al., 2011; Clemens et al., 2011). Earlier studies suggested that timing differences among cortical spindles reflect propagation along the RE rather than through intracortical pathways (Kim et al., 1995; Contreras et al., 1997c). Accordingly, spindles may propagate rostrally along the RE, progressively innervating different dorsal nuclei which project topographically to the cortex, generating spindles with different frequencies at different times in different locations.

Sleep spindles are mostly local

Spindles have been traditionally regarded as global thalamocortical events, but local spindles were reported during cortical spreading depression and barbiturate anesthesia (Andersen and Andersson, 1968; Contreras et al., 1996, 1997b,c). The current results demonstrate that most sleep spindles occur locally in natural sleep as do slow waves (Nir et al., 2011), and that local spindle occurrence does not simply reflect associations with slow waves or distinctions between slow and fast events. These findings suggest that spindles may occur or be regulated locally (Caderas et al., 1982; Nishida and Walker, 2007; Dehghani et al., 2010a; Halassa et al., 2011) and support the notion that sleep arises from activities of local circuits (Werth et al., 1997; Vyazovskiy et al., 2000; Huber et al., 2004, 2006; Esser et al., 2006; Krueger et al., 2008; Nir et al., 2011). It is an open question whether local and global spindles may be mediated by different mechanisms such as laminar-specific corticothalamic projections, or thalamocortical projections via the core and matrix cells (Zikopoulos and Barbas, 2007; Jones, 2009; Rubio-Garrido et al., 2009).

The relation of spindles with sleep slow waves

With respect to slow waves, spindles tend to occur preferentially at up-states (Mölle et al., 2002; Steriade, 2003). Such association has also been termed K-complex but this terminology is still under debate (Steriade and Amzica, 1998; Cash et al., 2009). Centroparietal spindles tend to occur shortly after the transition to up-states. Since up-states are believed to trigger spindles through

corticothalamic projections, centroparietal cortex may exert particularly powerful corticothalamic feedback. Given that slow waves propagate from prefrontal cortex toward posterior regions (Massimini et al., 2004; Nir et al., 2011), and spindles occur sooner in posterior regions (above), the net result is that frontal spindles occur later during slow-wave up-states.

Our results extend the notion of reciprocal relation between SWA and spindle frequency and density (Steriade and Amzica, 1998; Wei et al., 1999; Himanen et al., 2002; De Gennaro and Ferrara, 2003). In stage N3 when SWA is maximal, spindle density is reduced. In early NREM sleep when SWA is highest, spindle density and spindle frequency are significantly lower. Moreover, spindle density and frequency are lower in the middle of NREM cycles when SWA is maximal and higher toward the transition to REM sleep when SWA tapers off.

Unit discharges during sleep spindles

We found that firing rate modulations of cortical neurons during spindles are weak and unreliable compared with those observed during slow waves (Nir et al., 2011), largely consistent with previous reports (Evarts, 1964; Steriade et al., 1974; Sirota et al., 2003). This seems at odds with suggestions that sleep spindles play an important role in disconnection from the external environment or in memory consolidation (Diekelmann and Born, 2010) but perhaps specific neuronal populations are more strongly modulated during spindles (Dehghani et al., 2010b). Another possibility is that inhibition in NREM sleep may occur concomitantly with spindle-driven postsynaptic potentials in dendrites and prevent reliable spike firing (Contreras et al., 1997a).

In addition, we found that spindles affected spike timing in cortical neurons. The discharges of 20% of neurons were significantly phase-locked, firing maximally in the ascending slope of spindles in the depth EEG as in animal studies (Contreras and Steriade, 1996; Sirota et al., 2003). Interpretation of entrained neurons and their preferred phase should consider that unit discharges were recorded ~4 mm away from depth EEG and their laminar profiles remain unknown, which could explain minor differences with other species (Sirota et al., 2003; Dehghani et al., 2010b). That spike timing is modulated by sleep spindles and is also implicated in plasticity processes (Caporale and Dan, 2008) supports the notion that spindles may have a role in synaptic plasticity (Khazipov et al., 2004). A trend for higher firing rates in phase-locked units could suggest that specific cell types (e.g., inhibitory interneurons) preferentially modulate their spike timing with spindles, but our data could not resolve this intriguing possibility.

Spindle density and frequency as reflections of thalamic hyperpolarization

We suggest that the level of thalamic hyperpolarization may be a key factor governing multiple spindle properties such as their spectral frequency, density, regional variability, dynamics during individual events, and across sleep. In TC cells, the degree of hyperpolarization dictates the period of spindle oscillations (McCormick and Bal, 1997; Steriade, 2003). Along this line, we find that deeper sleep (higher SWA and presumably stronger thalamic hyperpolarization) is associated with lower frequency cortical spindles. In addition, at the level of individual thalamic neurons, spindles and slow waves arise at different hyperpolarization levels and are mutually exclusive (Nuñez et al., 1992). Indeed, we find that high SWA is associated with fewer spindles, presumably since strong hyperpolarization reduces the recruitment of thalamic neurons that support spindle generation. Regional differences in spindle density and frequency may stem from differential hyperpolarization levels in specific thalamic subregions. For example, posterior thalamic nuclei (projecting to centroparietal cortices) receive stronger cholinergic innervations (Jones, 2007). Alternatively, intrinsic cellular properties may differ regionally in thalamic and RE neurons (e.g., distributions of neurotransmitter receptors or ionic channels). Finally, deceleration during each spindle could reflect increasing hyperpolarization. Cortical neurons are increasingly more involved in spindle termination (Contreras et al., 1996; Steriade, 2003), and these corticothalamic projections are believed to exert an overall inhibitory influence through their strong influence on RE cells (Golshani et al., 2001). If this hypothesis is correct, a simple noninvasive EEG measure of spindle frequency could provide an important proxy for the level of thalamocortical polarization at any given time.

Notes

Supplemental material for this article is available at http://tononi.psychiatry.wisc.edu/pubs/spindles.pdf. Online supporting supplemental material (two tables and five figures) including recording details, clinical information and sleep study details, sleep architecture material, analysis of early vs late sleep epochs, spindle frequency distributions in each individual and depth electrode, unit identification and stability throughout sleep recordings, and spindles in the hippocampus and medial temporal lobe. This material has not been peer reviewed.

References

Achermann P, Borbely AA (1998) Temporal evolution of coherence and power in the human sleep electroencephalogram. J Sleep Res 7 [Suppl 1]:36–41.

Akkal D, Dum RP, Strick PL (2007) Supplementary motor area and presupplementary motor area: targets of basal ganglia and cerebellar output. J Neurosci 27:10659–10673.

Anderer P, Klösch G, Gruber G, Trenker E, Pascual-Marqui RD, Zeitlhofer J, Barbanoj MJ, Rappelsberger P, Saletu B (2001) Low-resolution brain electromagnetic tomography revealed simultaneously active frontal and parietal sleep spindle sources in the human cortex. Neuroscience 103:581–592.

Andersen P, Andersson S (1968) Physiological basis of the alpha rhythm. New York: Meridith.

Bal T, von Krosigk M, McCormick DA (1995) Synaptic and membrane mechanisms underlying synchronized oscillations in the ferret lateral geniculate nucleus in vitro. J Physiol 483:641–663.

Bonjean M, Baker T, Lemieux M, Timofeev I, Sejnowski T, Bazhenov M (2011) Corticothalamic feedback controls sleep spindle duration *in vivo*. J Neurosci 31:9124–9134.

Caderas M, Niedermeyer E, Uematsu S, Long DM, Nastalski J (1982) Sleep spindles recorded from deep cerebral structures in man. Clin Electroencephalogr 13:216–225.

Caporale N, Dan Y (2008) Spike timing-dependent plasticity: a Hebbian learning rule. Annu Rev Neurosci 31:25–46.

Cappe C, Morel A, Barone P, Rouiller EM (2009) The thalamocortical projection systems in primate: an anatomical support for multisensory and sensorimotor interplay. Cereb Cortex 19:2025–2037.

Cash SS, Halgren E, Dehghani N, Rossetti AO, Thesen T, Wang C, Devinsky O, Kuzniecky R, Doyle W, Madsen JR, Bromfield E, Eross L, Halász P, Karmos G, Csercsa R, Wittner L, Ulbert I (2009) The human K-complex represents an isolated cortical down-state. Science 324:1084–1087.

Clemens Z, Mölle M, Eross L, Barsi P, Halász P, Born J (2007) Temporal coupling of parahippocampal ripples, sleep spindles and slow oscillations in humans. Brain 130:2868–2878.

Clemens Z, Mölle M, Eross L, Jakus R, Rásonyi G, Halász P, Born J (2011) Fine-tuned coupling between human parahippocampal ripples and sleep spindles. Eur J Neurosci 33:511–520.

Contreras D, Steriade M (1996) Spindle oscillation in cats: the role of

corticothalamic feedback in a thalamically generated rhythm. J Physiol 490:159–179.
Contreras D, Destexhe A, Sejnowski TJ, Steriade M (1996) Control of spatiotemporal coherence of a thalamic oscillation by corticothalamic feedback. Science 274:771–774.
Contreras D, Destexhe A, Steriade M (1997a) Intracellular and computational characterization of the intracortical inhibitory control of synchronized thalamic inputs in vivo. J Neurophysiol 78:335–350.
Contreras D, Destexhe A, Steriade M (1997b) Spindle oscillations during cortical spreading depression in naturally sleeping cats. Neuroscience 77:933–936.
Contreras D, Destexhe A, Sejnowski TJ, Steriade M (1997c) Spatiotemporal patterns of spindle oscillations in cortex and thalamus. J Neurosci 17:1179–1196.
de Curtis M, Avanzini G (2001) Interictal spikes in focal epileptogenesis. Prog Neurobiol 63:541–567.
De Gennaro L, Ferrara M (2003) Sleep spindles: an overview. Sleep Med Rev 7:423–440.
Dehghani N, Cash SS, Chen CC, Hagler DJ Jr, Huang M, Dale AM, Halgren E (2010a) Divergent cortical generators of MEG and EEG during human sleep spindles suggested by distributed source modeling. PLoS One 5:e11454.
Dehghani N, Peyrache A, Destexhe A (2010b) Dynamics of excitation and inhibition, and local interactions, during slow wave sleep oscillations in rat prefrontal cortex. Soc Neurosci Abstr 36:44.5.
Dehghani N, Cash SS, Halgren E (2011) Topographical frequency dynamics within EEG and MEG sleep spindles. Clin Neurophysiol 122:229–235.
Destexhe A, Sejnowski TJ (2001) Thalamocortical assemblies: how ion channels, single neurons and large-scale networks organize sleep oscillations. Oxford: Oxford UP.
Destexhe A, Sejnowski TJ (2002) The initiation of bursts in thalamic neurons and the cortical control of thalamic sensitivity. Philos Trans R Soc Lond B Biol Sci 357:1649–1657.
Destexhe A, Contreras D, Steriade M (1998) Mechanisms underlying the synchronizing action of corticothalamic feedback through inhibition of thalamic relay cells. J Neurophysiol 79:999–1016.
Diekelmann S, Born J (2010) The memory function of sleep. Nat Rev Neurosci 11:114–126.
Dinner DS, Lüders HO, eds (2001) Epilepsy and sleep: physiological and clinical relationships. San Diego: Academic.
Esser SK, Huber R, Massimini M, Peterson MJ, Ferrarelli F, Tononi G (2006) A direct demonstration of cortical LTP in humans: a combined TMS/EEG study. Brain Res Bull 69:86–94.
Evarts EV (1964) Temporal patterns of discharge of pyramidal tract neurons during sleep and waking in the monkey. J Neurophysiol 27:152–171.
Ferrarelli F, Huber R, Peterson MJ, Massimini M, Murphy M, Riedner BA, Watson A, Bria P, Tononi G (2007) Reduced sleep spindle activity in schizophrenia patients. Am J Psychiatry 164:483–492.
Ferrarelli F, Peterson MJ, Sarasso S, Riedner BA, Murphy MJ, Benca RM, Bria P, Kalin NH, Tononi G (2010) Thalamic dysfunction in schizophrenia suggested by whole-night deficits in slow and fast spindles. Am J Psychiatry 167:1339–1348.
Fried I, Wilson CL, Maidment NT, Engel J Jr, Behnke E, Fields TA, MacDonald KA, Morrow JW, Ackerson L (1999) Cerebral microdialysis combined with single-neuron and electroencephalographic recording in neurosurgical patients. Technical note. J Neurosurg 91:697–705.
Gibbs FA, Gibbs EL (1950) Atlas of electroencephalography. Boston: Addison-Wesley.
Golshani P, Liu XB, Jones EG (2001) Differences in quantal amplitude reflect GluR4-subunit number at corticothalamic synapses on two populations of thalamic neurons. Proc Natl Acad Sci U S A 98:4172–4177.
Guillery RW, Harting JK (2003) Structure and connections of the thalamic reticular nucleus: advancing views over half a century. J Comp Neurol 463:360–371.
Halassa MM, Siegle JH, Ritt JT, Ting JT, Feng G, Moore CI (2011) Selective optical drive of thalamic reticular nucleus generates thalamic bursts and cortical spindles. Nat Neurosci 14:1118–1120.
Himanen SL, Virkkala J, Huhtala H, Hasan J (2002) Spindle frequencies in sleep EEG show U-shape within first four NREM sleep episodes. J Sleep Res 11:35–42.
Huber R, Ghilardi MF, Massimini M, Tononi G (2004) Local sleep and learning. Nature 430:78–81.
Huber R, Ghilardi MF, Massimini M, Ferrarelli F, Riedner BA, Peterson MJ, Tononi G (2006) Arm immobilization causes cortical plastic changes and locally decreases sleep slow wave activity. Nat Neurosci 9:1169–1176.
Iber C, Ancoli-Israel S, Chesson AL, Quan SF (2007) AASM manual for the scoring of sleep and associate events. Rules, terminology and technical specifications. Westchester, IL: American Association of Sleep Medicine.
Jankel WR, Niedermeyer E (1985) Sleep spindles. J Clin Neurophysiol 2:1–35.
Jobert M, Poiseau E, Jähnig P, Schulz H, Kubicki S (1992) Topographical analysis of sleep spindle activity. Neuropsychobiology 26:210–217.
Jones EG (2002) Thalamic circuitry and thalamocortical synchrony. Philos Trans R Soc Lond B Biol Sci 357:1659–1673.
Jones EG (2007) The thalamus, Ed 2. Cambridge, UK: Cambridge UP.
Jones EG (2009) Synchrony in the interconnected circuitry of the thalamus and cerebral cortex. Ann N Y Acad Sci 1157:10–23.
Khazipov R, Sirota A, Leinekugel X, Holmes GL, Ben-Ari Y, Buzsáki G (2004) Early motor activity drives spindle bursts in the developing somatosensory cortex. Nature 432:758–761.
Kim U, Bal T, McCormick DA (1995) Spindle waves are propagating synchronized oscillations in the ferret LGNd in vitro. J Neurophysiol 74:1301–1323.
Krueger JM, Rector DM, Roy S, Van Dongen HP, Belenky G, Panksepp J (2008) Sleep as a fundamental property of neuronal assemblies. Nat Rev Neurosci 9:910–919.
Lam YW, Sherman SM (2011) Functional organization of the thalamic input to the thalamic reticular nucleus. J Neurosci 31:6791–6799.
Loomis AL, Harvey EN, Hobart G (1935) Potential rhythms of the cerebral cortex during sleep. Science 81:597–598.
Lüthi A, McCormick DA (1998) Periodicity of thalamic synchronized oscillations: the role of Ca^{2+}-mediated upregulation of Ih. Neuron 20:553–563.
Malow BA, Carney PR, Kushwaha R, Bowes RJ (1999) Hippocampal sleep spindles revisited: physiologic or epileptic activity? Clin Neurophysiol 110:687–693.
Marini G, Macchi G, Mancia M (1992) Potentiation of electroencephalographic spindles by ibotenate microinjections into nucleus reticularis thalami of cats. Neuroscience 51:759–762.
Massimini M, Huber R, Ferrarelli F, Hill S, Tononi G (2004) The sleep slow oscillation as a traveling wave. J Neurosci 24:6862–6870.
McCormick DA, Bal T (1997) Sleep and arousal: thalamocortical mechanisms. Annu Rev Neurosci 20:185–215.
Mölle M, Marshall L, Gais S, Born J (2002) Grouping of spindle activity during slow oscillations in human non-rapid eye movement sleep. J Neurosci 22:10941–10947.
Morison RS, Bassett DI (1945) Electrical activity of the thalamus and basal ganglia in decorticated cats. J Neurophysiol 8:309–314.
Nakabayashi T, Uchida S, Maehara T, Hirai N, Nakamura M, Arakaki H, Shimisu H, Okubo Y (2001) Absence of sleep spindles in human medial and basal temporal lobes. Psychiatry Clin Neurosci 55:57–65.
Nakamura M, Uchida S, Maehara T, Kawai K, Hirai N, Nakabayashi T, Arakaki H, Okubo Y, Nishikawa T, Shimizu H (2003) Sleep spindles in human prefrontal cortex: an electrocorticographic study. Neurosci Res 45:419–427.
Nir Y, Mukamel R, Dinstein I, Privman E, Harel M, Fisch L, Gelbard-Sagiv H, Kipervasser S, Andelman F, Neufeld MY, Kramer U, Arieli A, Fried I, Malach R (2008) Interhemispheric correlations of slow spontaneous neuronal fluctuations revealed in human sensory cortex. Nat Neurosci 11:1100–1108.
Nir Y, Staba RJ, Andrillon T, Vyazovskiy VV, Cirelli C, Fried I, Tononi G (2011) Regional slow waves and spindles in human sleep. Neuron 70:153–169.
Nishida M, Walker MP (2007) Daytime naps, motor memory consolidation and regionally specific sleep spindles. PLoS One 2:e341.
Nuñez A, Curro Dossi R, Contreras D, Steriade M (1992) Intracellular evidence for incompatibility between spindle and delta oscillations in thalamocortical neurons of cat. Neuroscience 48:75–85.
Paré D, Steriade M, Deschênes M, Oakson G (1987) Physiological characteristics of anterior thalamic nuclei, a group devoid of inputs from reticular thalamic nucleus. J Neurophysiol 57:1669–1685.
Paré D, Collins DR, Pelletier JG (2002) Amygdala oscillations and the consolidation of emotional memories. Trends Cogn Sci 6:306–314.
Quiroga RQ, Nadasdy Z, Ben-Shaul Y (2004) Unsupervised spike detection

and sorting with wavelets and superparamagnetic clustering. Neural Comput 16:1661–1687.

Riedner BA, Vyazovskiy VV, Huber R, Massimini M, Esser S, Murphy M, Tononi G (2007) Sleep homeostasis and cortical synchronization: III. A high-density EEG study of sleep slow waves in humans. Sleep 30:1643–1657.

Rubio-Garrido P, Pérez-de-Manzo F, Porrero C, Galazo MJ, Clascá F (2009) Thalamic input to distal apical dendrites in neocortical layer 1 is massive and highly convergent. Cereb Cortex 19:2380–2395.

Schabus M, Gruber G, Parapatics S, Sauter C, Klösch G, Anderer P, Klimesch W, Saletu B, Zeitlhofer J (2004) Sleep spindles and their significance for declarative memory consolidation. Sleep 27:1479–1485.

Schabus M, Dang-Vu TT, Albouy G, Balteau E, Boly M, Carrier J, Darsaud A, Degueldre C, Desseilles M, Gais S, Phillips C, Rauchs G, Schnakers C, Sterpenich V, Vandewalle G, Luxen A, Maquet P (2007) Hemodynamic cerebral correlates of sleep spindles during human non-rapid eye movement sleep. Proc Natl Acad Sci U S A 104:13164–13169.

Siapas AG, Lubenov EV, Wilson MA (2005) Prefrontal phase locking to hippocampal theta oscillations. Neuron 46:141–151.

Sirota A, Csicsvari J, Buhl D, Buzsáki G (2003) Communication between neocortex and hippocampus during sleep in rodents. Proc Natl Acad Sci U S A 100:2065–2069.

Steriade M (2000) Corticothalamic resonance, states of vigilance and mentation. Neuroscience 101:243–276.

Steriade M (2003) Neuronal substrates of sleep and epilepsy, Ed 1. Cambridge, UK: Cambridge UP.

Steriade M (2005) Sleep, epilepsy and thalamic reticular inhibitory neurons. Trends Neurosci 28:317–324.

Steriade M, Amzica F (1998) Coalescence of sleep rhythms and their chronology in corticothalamic networks. Sleep Res Online 1:1–10.

Steriade M, Timofeev I (2003) Neuronal plasticity in thalamocortical networks during sleep and waking oscillations. Neuron 37:563–576.

Steriade M, Deschênes M, Oakson G (1974) Inhibitory processes and interneuronal apparatus in motor cortex during sleep and waking. I. Background firing and responsiveness of pyramidal tract neurons and interneurons. J Neurophysiol 37:1065–1092.

Steriade M, Parent A, Hada J (1984) Thalamic projections of nucleus reticularis thalami of cat: a study using retrograde transport of horseradish peroxidase and fluorescent tracers. J Comp Neurol 229:531–547.

Steriade M, Deschênes M, Domich L, Mulle C (1985) Abolition of spindle oscillations in thalamic neurons disconnected from nucleus reticularis thalami. J Neurophysiol 54:1473–1497.

Steriade M, Domich L, Oakson G, Deschênes M (1987) The deafferented reticular thalamic nucleus generates spindle rhythmicity. J Neurophysiol 57:260–273.

Steriade M, Nuñez A, Amzica F (1993a) Intracellular analysis of relations between the slow (<1 Hz) neocortical oscillation and other sleep rhythms of the electroencephalogram. J Neurosci 13:3266–3283.

Steriade M, Contreras D, Curró Dossi R, Nuñez A (1993b) The slow (<1 Hz) oscillation in reticular thalamic and thalamocortical neurons: scenario of sleep rhythm generation in interacting thalamic and neocortical networks. J Neurosci 13:3284–3299.

Timofeev I, Grenier F, Steriade M (2001) Disfacilitation and active inhibition in the neocortex during the natural sleep-wake cycle: an intracellular study. Proc Natl Acad Sci U S A 98:1924–1929.

von Krosigk M, Bal T, McCormick DA (1993) Cellular mechanisms of a synchronized oscillation in the thalamus. Science 261:361–364.

Vyazovskiy V, Borbély AA, Tobler I (2000) Unilateral vibrissae stimulation during waking induces interhemispheric EEG asymmetry during subsequent sleep in the rat. J Sleep Res 9:367–371.

Wei HG, Riel E, Czeisler CA, Dijk DJ (1999) Attenuated amplitude of circadian and sleep-dependent modulation of electroencephalographic sleep spindle characteristics in elderly human subjects. Neurosci Lett 260:29–32.

Werth E, Achermann P, Borbély AA (1997) Fronto-occipital EEG power gradients in human sleep. J Sleep Res 6:102–112.

Zepelin H, Siegel JM, Tobler I (1994) Mammalian sleep. In: Principles and practice of sleep medicine (Kryger MH, Roth T, Dement WC, eds), pp 91–100. London: Saunders.

Zhang D, Snyder AZ, Shimony JS, Fox MD, Raichle ME (2010) Noninvasive functional and structural connectivity mapping of the human thalamocortical system. Cereb Cortex 20:1187–1194.

Zikopoulos B, Barbas H (2007) Parallel driving and modulatory pathways link the prefrontal cortex and thalamus. PLoS One 2:e848.

Zygierewicz J, Blinowska KJ, Durka PJ, Szelenberger W, Niemcewicz S, Androsiuk W (1999) High resolution study of sleep spindles. Clin Neurophysiol 110:2136–2147.